JOURNAL OF MATERIALS SCIENCE 30 (1995) 3591–3597

Microstructural evolution of FINEMET type alloys with chromium: An electron microscopy study

M. MILLÁN, C. F. CONDE, A. CONDE
Departamento de Física de la Materia Condensada, Instituto de Ciencia de Materiales, CSIC-Universidad de Sevilla, Apartado 1065, 41080-Sevilla, Spain

Microstructural changes in $Fe_{73.5-x}Cr_xCu_1Nb_3Si_{13.5}B_9$ ($0 \leqslant x \leqslant 5$) alloys with thermal treatment were studied by electron microscopy. In a first stage, around 800 K, an Fe(Si) nanocrystalline phase is formed in the amorphous residual matrix. Crystallization onset is enhanced with the Cr content of the alloy. In a second stage, around 950 K, full crystallization of the samples leads to the formation of a body centred cubic (b.c.c.) boride-type unknown crystal phase with a lattice parameter of $a = 1.52$ nm, and recrystallization of the previous Fe(Si) nanophase also occurs. No qualitative differences were found between dynamic and isothermal crystallization. The size effect for thin samples is limited to a lowering of crystallization temperatures. For isothermal nanocrystallization in the temperature range 775–900 K, the mean grain size of the nanocrystals increases for short annealing times to stabilize at a constant value of about 10–15 nm for long annealing times. The stabilized grain size increases with increasing annealing temperature and slightly decreases with the Cr content of the alloy.

1. Introduction

Nanocrystalline materials consist of two main structural components: small crystals, of 5–30 nm in size, randomly dispersed in an amorphous matrix. The grain boundaries are part of this amorphous rest phase, the "amorphous grain boundary phase", and play an important role in the physical properties of the nanometer sized solids, since their volume fraction is much larger than in polycrystalline materials.

Recently, it has been found that it is possible to obtain bulk ultrafine grain structures by controlled crystallization of metallic glasses [1–5]. The excellent soft magnetic properties of the properly annealed iron-based amorphous alloy of $Fe_{73.5}Cu_1Nb_3Si_{13.5}B_9$ composition, denoted as FINEMET [1, 2], have particularly attracted great scientific interest in these alloys.

The soft magnetic properties of FINEMET alloys are attributed to the ultrafine grain structure of Fe(Si) crystals, in the 10–20 nm size range, revealed after annealing at about 850 K [6, 7]. The existence and thermal stability of this microstructure are attributed to the presence of Cu and Nb in these alloys. Since copper is virtually insoluble in iron, it has been speculated that the inhomogeneity of Cu occurs at an initial stage of crystallization, which causes an increased number of nucleation sites of the iron phase. However, as proposed by Köster *et al.* [5], only small additions of Cu atoms to the alloy lead to an increase in "quenched-in" nucleation sites, which accelerate the nucleation of the primary crystallization. On the other hand, the addition of niobium atoms to the alloy retards the grain growth during crystallization because Nb inhibits the diffusion of the Si and B atoms and, therefore, the increase in grain size is limited to about 10 nm in diameter. So, the combined addition of Cu and Nb results in the formation of an ultrafine grain structure [1, 5].

Crystallization processes in Fe–Cu–Nb–Si–B have been extensively studied by different experimental techniques [8–16]. Two crystallization stages are detected before the final stable phases are attained. The first process, with onset at about 800 K, corresponds to the segregation of an Fe(Si) cubic nanophase; other phases crystallize at higher temperatures (~ 875 K). However, most of the published works refer to the nanocrystallization stage, though crystallization behaviour on extended heat treatment is not definitely known.

The aim of this work has been to study by transmission electron microscopy (TEM) the microstructure evolution in FINEMET alloys containing chromium, in the course of the crystallization process up to the final stable phases. Recently [17], the authors have reported a thermomagnetic study of devitrification in these alloys.

2. Experimental procedure

Ribbons, approximately 5 mm wide and 25 μm thick, of alloys with nominal compositions of $Fe_{73.5-x}Cr_x$-$Cu_1Nb_3Si_{13.5}B_9$ ($0 \leqslant x \leqslant 5$) were prepared by a

0022–2461

melt spinning technique. The amorphous character of as-quenched samples was checked by X-ray diffraction (XRD).

Specimens for TEM studies were prepared by using a twin-jet electrochemical polishing device with a 10% perchloric acid–acetic acid solution. To allow correlation of TEM observations with results of other experimental techniques, such as differential scanning calorimetry (DSC) and thermomagnetic gravimetry (TMG), samples were heat treated in the DSC chamber before thinning. TEM observations were performed on an Hitachi H-800 electron microscope with an accelerating voltage of 200 kV. For some observations a specimen heating holder was used to heat the foils resistively into the TEM chamber during observation. Bright field and dark field images and selected area electron diffraction (SAD) patterns, were recorded throughout the study.

3. Results

The authors' previously reported results [17] derived from DSC dynamic experiments showed that the devitrification process in the studied alloys occurs in two stages, at temperatures indicated in Table I. In the first stage, the Fe(Si) nanophase is formed and a residual amorphous FeB rich phase remains. After the second crystallization stage, thermomagnetic results indicate the existence, at least, of two magnetic phases: an Fe(Si) with a lower content of Si, as indicated by the Curie temperature value, and another boride type unknown phase.

3.1. Dynamic crystallization

For as-quenched samples only the homogeneous mazy contrast, which is known to be characteristic of an amorphous structure, is observed in TEM images of all the alloys studied (Fig. 1a). No indication of the presence of microcrystallites was observed and the electron diffraction pattern shows only diffuse haloes.

Samples studied in this section were partially crystallized in the DSC chamber, by interrupting the heating run at different temperatures selected from previous results (Table I) for the different alloys.

For samples heated up to about 800 K (an intermediate temperature between the onset and the peak temperatures of the first DSC exotherm for each alloy), TEM images (Fig. 1b) reveal the presence of a low density of nanocrystals, with an average grain size of 5–10 nm, randomly dispersed in the matrix. The SAD pattern indicates that the observed nanocrystalline phase should correspond to a supersaturated solid solution, α-Fe(Si). Diffuse haloes in the electron diffraction pattern indicate that the amorphous phase is still present, as it is also clearly visible in TEM images.

For samples heated up to about 900 K (an intermediate temperature between the two DSC exotherms), TEM images (Fig. 1c) reveal an increase of the crystallized volume fraction: a higher density of nanocrystals is observed and also the grain size has increased to about 10–15 nm. Grains seem to be surrounded by the remanent amorphous matrix and impingement of grains is not particularly important. Progress in the nanocrystallization reaction is also evidenced by increasing intensity of the sharp crystal lines in the diffraction pattern. The presence of halo traces in the SAD pattern confirms that the crystallization reaction is not yet complete.

The presence, at the end of the first crystallization stage, of the crystalline iron–silicon nanophase, as well as the amorphous rest phase, with a reduced content of iron and silicon is generally accepted in the published studies of FINEMET alloys. Mean grain sizes in the range 10–20 nm have been reported [6, 8, 10, 18] for Fe(Si) nanocrystals, having a DO_3 structure of Fe_3Si [8, 19] and a silicon content of 15–25 at % [6, 10, 17, 18, 20], as derived from the lattice parameter or Curie temperature values, Mossbauer results, etc. In fact, only up to 10 at % Si is soluble in b.c.c. Fe and the ordered structure DO_3 exists for the range 10–30 at% Si [21]; the lattice parameter depending linearly on silicon content. The amorphous matrix mainly consists of Fe–Nb–B and the balance of atomic concentration should indicate compositions of typically $F_{(bal)}Nb_{(5-10)}B_{\sim 30}$ at % [22].

Values obtained for the lattice parameter of the b.c.c. cell of the Fe(Si) phase, in spite of the limited accuracy attainable from standard electron diffraction patterns, show an increase in the course of the heat treatment: from 0.283 nm for samples heated up to ~800 K, to 0.286 nm for samples heated up to ~900 K. This variation of the cell constant, in agreement with those previously reported from X-ray diffraction data, should be related to the change of the silicon content in the nanocrystalline Fe(Si) phase: a decreasing silicon content leads to an increase of the lattice cell constant, depending linearly on silicon concentration.

Thus, according to the data in [21], the lattice parameter found values should correspond to about 20–22 at % for samples heated up to ~800 K and 5–10 at % for samples heated up to ~900 K. These TEM results on the silicon content of the Fe(Si) nanocrystals are in close agreement with those obtained from TMG measurements on the same alloys [17], derived from the Curie temperature values of the iron nanophase.

TEM observations on samples of the different composition alloys do not reveal qualitative changes in the nanocrystallization process, except for variation in the crystallization onset temperature, slightly shifted to higher temperatures upon increasing Cr content (Table I). No significant changes are found with respect to the mean size of nanocrystals and the lattice

TABLE I Crystalization temperatures for $Fe_{73.5-x}Cr_xCu_1Nb_3Si_{13.5}B_9$ alloys derived from DSC results [17]

	$x=0$	$x=1$	$x=2$	$x=3$	$x=4$	$x=5$
T_{p1} (K)	806	808	816	819	822	825
T_{p2} (K)	954	968	974	963	967	968

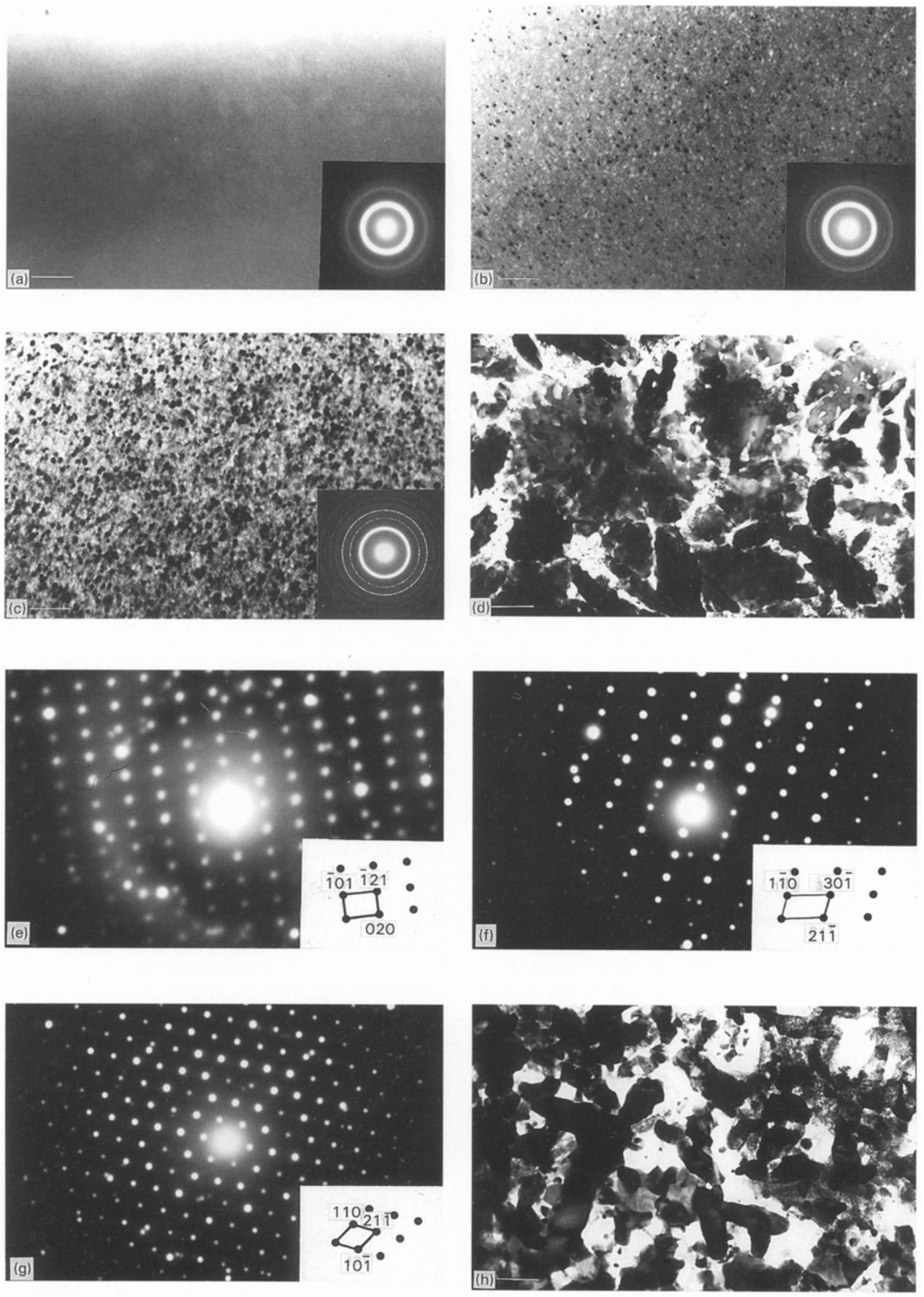

Figure 1 Dynamic crystallization process for sample of the 2 at % Cr alloy: (a) as-cast amorphous sample; (b) early stage of nanocrystallization in a sample heated up to 800 K; (c) nanocrystals in a sample heated up to 900 K; (d) fully crystallized sample (heated up to 1000 K) showing the large crystals of the boride type phase and the recrystallized Fe(Si) grains; (e)–(g) diffraction patterns of b.c.c. boride type structure; (h) sample annealed at 1100 K. (Bar = 100 nm for (a), (b), and (c) and 200 nm for (d) and (h).)

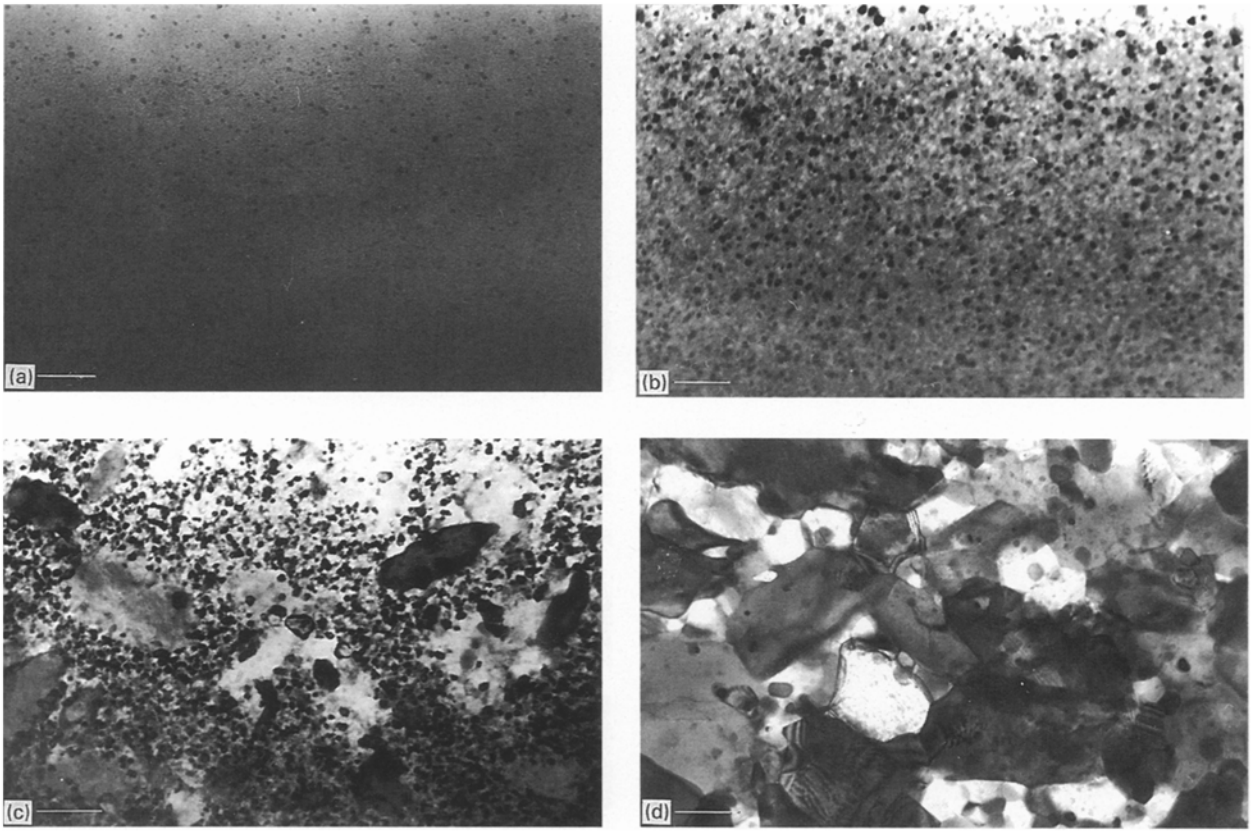

Figure 2 Crystallization in the electron microscope of 5 at % Cr alloy samples: (a) early crystallization stage, around 725 K; (b) progress in the nanocrystallization reaction at about 850 K; (c) second stage of the crystallization on heating up to 975 K; (d) microstructure after annealing at 1075 K. (Bar = 100 nm for (a) and (b), and 150 nm for (c) and (d).)

parameter value (related to the silicon content). This last result agrees with previous magnetic results [17]: the Curie temperature of the Fe(Si) nanophase is not dependent on the Cr content of the alloy and this suggests that Cr should be excluded from the nanocrystals.

Heating of the samples up to 1000 K (after the end of the second DSC exotherm) leads to full crystallization of the remaining amorphous matrix (Fig. 1d). Recrystallization of the Fe(Si) phase is also observed: the ultrafine grain structure of the iron–silicon phase turns into a coarse grained one. As can be seen, a small number of abnormally large grains are produced by secondary crystallization due to rapid extension of a few grain boundary fronts. Fig. 1e to g shows selected area diffraction patterns of different reciprocal lattice sections of these grains. The interpretation of these patterns leads to an unknown b.c.c. structure with a lattice parameter of $a = 1.52$ nm. This phase has not been found in previous publications on crystallization of FINEMET alloys, only Duhaj *et al.* [23] reported the existence of electron diffraction patterns implying a cubic structure which could be indexed as b.c.c. or face centred cubic (f.c.c.), with a lattice constant of $a = 0.9$–1.8 nm.

Finally, for samples heated up to 1100 K and annealed at this temperature, TEM images (Fig. 1h) show the coexistence of different sized grains. Electron diffraction patterns reveal that the main phases present are the above cited b.c.c. phase with $a = 1.52$ nm and the $Fe_3Nb_4Si_5$ orthorhombic phase ($a = 1.2821$, $b = 0.4912$, $c = 1.5521$ nm). Besides these main phases, other diffraction patterns observed should indicate an *L*-lattice orthorhombic phase related to the above $Fe_3Nb_4Si_5$ (by tripling the *b* parameter) and also a polycrystalline pattern of a small grain size f.c.c. phase with a lattice parameter of $a = 0.362$ nm that should correspond to copper crystals. The presence of elementary copper is consistent with the model of preliminary Cu precipitation as the origin of the Fe(Si) enhanced nucleation.

FINEMET alloys annealed at temperatures of between 900 and 1100 K have been the subject of multiple phase analyses and a number of different crystalline phases are reported. However, only the existence of the DO_3–Fe–Si phase is commonly accepted, whereas different borides and related structures are reported in the publications: Fe_2B [13, 14, 24, 25], Fe_3B [13, 25], $(Fe,Si)_3B$ [10, 14], $Fe_3(Si,B)$ [26], $Fe_{23}B_6$ [27], Fe–Nb–Si [14], etc. In the present study, these phases were not detected throughout the high number of analysed electron diffraction patterns, except a few for $Fe_3(Si,B)$.

3.2. *In situ* crystallized samples

As-cast amorphous samples, after thinning, were crystallized by dynamic heating inside the microscope chamber, at a heating rate of 10 K min^{-1}. The nominal temperature, which may be somewhat different from the actual temperature in the observed area of the sample, was measured by a Pt/Pt–Rh thermocouple.

Fig. 2a illustrates the early crystallization stage, around 725 K, with a low density of Fe(Si) nanocrystals

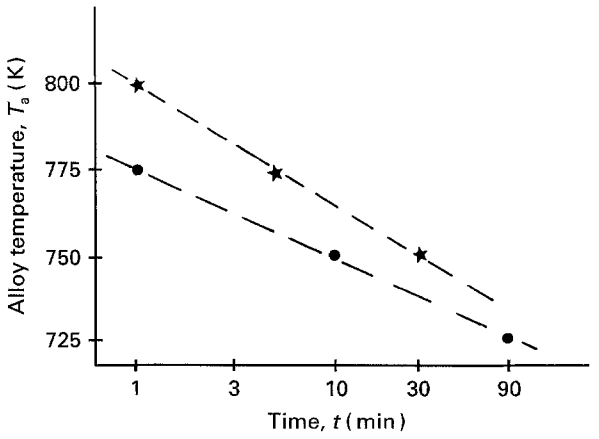

Figure 3 Time–temperature transition diagram for two different alloy compositions: (●) without Cr, and (★) 5 at % Cr. The enhancement of the crystallization time–temperature with Cr content is shown.

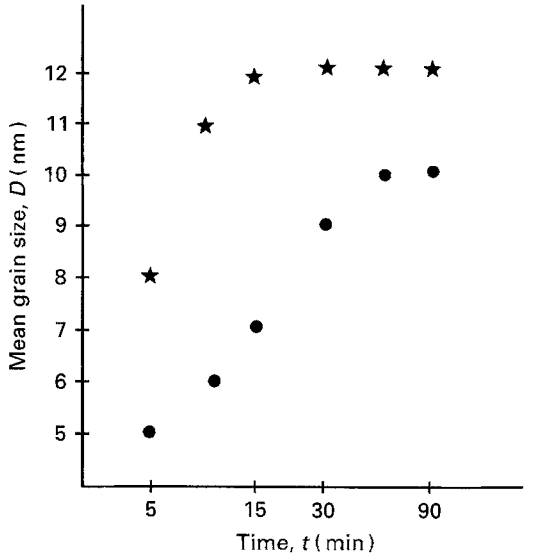

Figure 4 Mean grain size against annealing time for the alloy containing 2 at % Cr for annealing temperatures of (●) 775, and (★) 875 K. The grain size initially increases to be stabilized at a constant value for long times.

uniformly distributed in the amorphous matrix. No qualitative morphological changes are found with respect to the crystallization in bulk samples (Fig. 1b), except for the expected size effect, lowering the crystallization onset temperature by about 60 K.

Fig. 2b corresponds to a temperature of about 850 K and, as can be observed, the nanocrystallization reaction is in progress. Increase in the crystallized fraction is mainly due to the higher density of nanocrystals, but the mean grain size is also increased. Electron diffraction patterns, at this stage, show only the characteristic rings of the cubic Fe(Si) phase, along with a residual halo indicating the existence of an amorphous rest phase.

Fig. 2c shows a more advanced stage of the crystallization transformation, around 975 K. Two types of crystals are present: spheroidal type Fe(Si) nanocrystals and others of elongated form and significantly larger in size. Diffraction patterns reveal the existence of the two main phases described in Section 3.1.: the Fe(Si) phase and the b.c.c. boride type with unknown precise composition and lattice parameter $a = 1.52$ nm.

Finally, Fig. 2d shows the crystallite morphology of a sample heated up to 1075 K and annealed at this temperature for 1 h. The observed microstructure exhibits the polygonal forms usually found at the final crystallization stages of metallic glasses. The significantly uniform grain size of the different crystals should be noted, indicating a recrystallization reaction of the previous Fe(Si) nanophase. Electron diffraction patterns reveal the presence, as the main phases, of the two cubic phases previously cited, but, as reported in Section 3.1, some other minor phases are also found.

3.3. Isothermal nanocrystallization

In this section the authors report the results obtained from bulk samples isothermally annealed at temperatures in the range 725–900 K. After annealing for a certain period in the DSC chamber, cooling was achieved quickly to room temperature and after that samples were thinned for TEM observations.

Results of thermal stability of the amorphous alloys against nanocrystallization are illustrated in the time–temperature transition diagram shown in Fig. 3. As observed, the annealing time for the beginning of the nanophase formation largely increases below 750 K, whereas it is extremely short for temperatures above 800 K. On the other hand, with increasing Cr content of the alloy the nanocrystallization time–temperature values are enhanced.

For annealing temperatures in the explored range the mean grain size is found to be between 5 and 12 nm, depending on annealing conditions and composition of the alloy. These results agree with previously reported values for the mean grain size of nanocrystals in FINEMET type alloys, derived from TEM observations [6, 10, 12] or X-ray diffraction [8, 13, 28]. Fig. 4 illustrates the time dependence of the nanocrystal mean size for the two annealing temperatures. In the first short times (< 5–10 min) the mean grain size increases rapidly with increasing annealing time, to stabilize at a constant value for times greater than about 15–20 min. Increase of the annealing temperature leads to enhancement of the stabilized grain size of the nanocrystals. Thus, it is shown that the nanocrystalline Fe(Si) phase is stable in all the explored temperature range. On the other hand, increasing the Cr content of the alloy slightly lowers the mean grain size of the nanocrystals.

Fig. 5a–c correspond to samples of the alloy containing 2 at % Cr isothermally annealed at 775 K. At an early stage of nanocrystallization, TEM images (Fig. 5a) show a distribution of nanocrystals with a mean size of about 5 nm in the amorphous matrix. After annealing for 30 min (Fig. 5b) a higher density of nanocrystals is observed and also their mean grain size is increased to about 10 nm. After annealing for more than 60 min, the microstructure is stabilized as shown in Fig. 5c, corresponding to an annealing time of 120 min. Diffraction patterns at this stage reveal

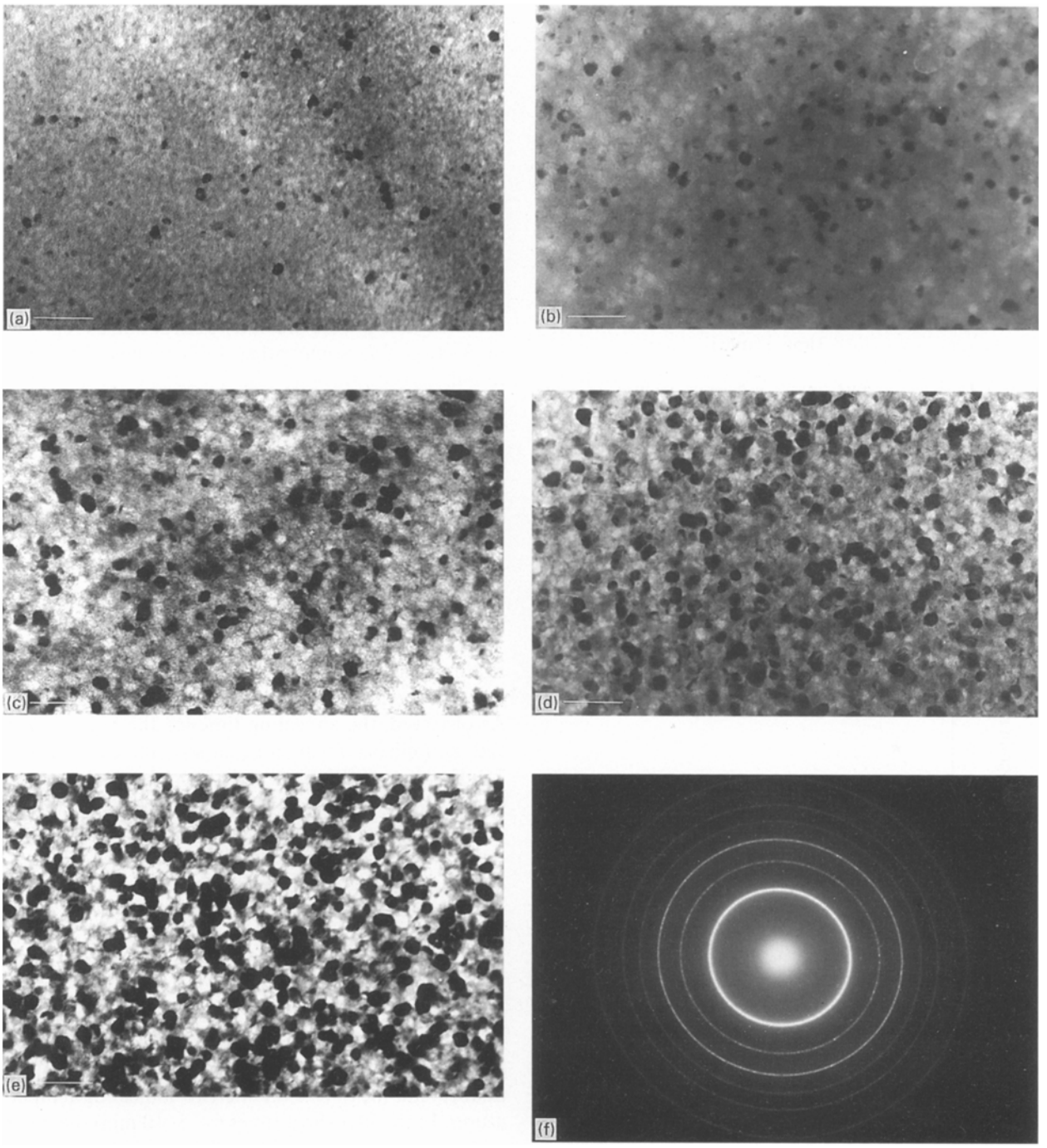

Figure 5 Isothermal nanocrystallization of two different composition alloys: (a)–(c) samples of the alloy containing 2 at % Cr annealed at 775 K for 5, 30 and 120 min, respectively; (d) and (e) samples of 5 at % Cr alloy annealed at 875 K for 5 and 90 min, respectively; (f) diffraction pattern of Fig. 5e. (Bar = 50 nm).

only the characteristic rings of the Fe(Si) nanophase and the residual of the amorphous rest phase.

Fig. 5d–f correspond to samples of the alloy with 5 at % Cr, isothermally annealed at 875 K. After an annealing time of 5 min (Fig. 5d), an advanced stage of the nanophase formation is observed, corresponding to a highly crystallized volume fraction. The mean grain size of the nanocrystals have reached the stabilized value of ~ 8 nm. For samples annealed for 90 min (Fig. 5e), only small qualitative changes are observed in the microstructure, but the mean grain size has increased to ~ 12 nm. Only a somewhat more significant impingement of grains is detected, but no other crystal types are evidenced. Diffraction patterns at this stage (Fig. 5f) confirm the presence of the Fe(Si) nanophase as the only crystal phase, and the low intensity halo evidences that the residual amorphous phase is still present.

As described above, the alloy composition does not produce qualitative changes in the nanocrystallization process and only an enhancement of the crystallization time–temperature and a slight lowering of the stabilized mean grain size of the nanocrystals should be noted.

Acknowledgements

The authors thank Dr A. Rodríguez-Pierna of the Basque Country University for kindly supplying the sample ribbons. They are also indebted to S. Velázquez for his assistance in photographic reproductions.

This work is supported by the CICYT of the Spanish Government (Project MAT92–718) and by the "Plan Andaluz de Investigación" of the Junta de Andalucía.

References

1. Y. YOSHIZAWA, S. OGUMA and K. YAMAUCHI, *J. Appl. Phys.* **64** (1988) 6044.
2. Y. YOSHIZAWA, K. YAMAUCHI, T. YAMANA and H. SUGIHAWA, *ibid.* **64** (1988) 6047.
3. K. LU, J. T. WANG and W. D. WEI, *ibid.* **69** (1991) 522.
4. R. LUCK, K. LU and W. FRANTZ, *Scripta Metall. et Mater.* **28** (1993) 1071.
5. U. KÖSTER, U. SCHÜNEMANN, M. BLANK-BEWERSDORFF, K. BRAUER, M. SUTTON and G. B. STEPHENSON, *Mater. Sci. Engng* **A133** (1991) 611.
6. G. HERZER, *IEEE Trans. Magn.* **25** (1989) 3327.
7. *Idem, Mater. Sci. Engng* **A133** (1991) 1.
8. M. MÜLLER, N. MATTERN and L. ILLGEN, *Z. Metallkde* **82** (1991) 895.
9. K. HIRAGA and O. KOHMOTO, *Mater. Trans.* **33** (1991) 868.
10. P. DUHAJ, P. SVEC, D. JANICKOVIC, I. MATKO and M. HLASNIK, *Mater. Sci. Engng* **B14** (1992) 357.
11. K. HONO, K. HIRAGA, Q. WANG, A. INOUE and T. SAKURAI, *Acta Metall. et Mater.* **40** (1992) 263.
12. G. HERZER and H. WARLIMONT, *NanoStruct. Mater.* **1** (1992) 263.
13. G. HAMPEL, A. PUNDT and J. HESSE, *J. Phys.: Condens. Matter* **4** (1992) 395.
14. G. RIXECKER, P. SCHAAF and U. GONSER, *ibid.* 4 (1992) 10295.
15. M. KNOBEL, D. R. SANTOS, I. L. TORRIANI and R. S. TURTELLI, *NanoStruct. Mater.* **2** (1993) 399.
16. X. D. LIU and J. T. WANG, *ibid.* **2** (1993) 63.
17. C. F. CONDE, M. MILLÁN and A. CONDE, *J. Magn. Magn. Mater.* **138** (1994) 314.
18. J. JIANG, F. AUBERTIN, U. GONSER and H. R. HILZINGER, *Z. Metallkde* **82** (1991) 698.
19. T. SAWA and Y. TAKAMASHI, *J. Appl. Phys.* **67** (1990) 5565.
20. T. ZEMCIK, Y. JIRÁSKOVÁ, K. ZAVETA, D. ECKERT, J. SCHNEIDER, N. MATTERN and D. HESSKE, *Mater. Lett.* **10** (1991) 313.
21. W. B. PEARSON, "A Handbook of the Lattice Spacing and Structures of Metals and Alloys" (Pergamon Press, London, 1958).
22. G. HERZER, *J. Magn. Magn. Mater.* **112** (1992) 258.
23. P. DUHAJ, P. SVEC, D. JANICKOVIC and I. MATKO, *Mater. Sci. Engng* **A133** (1991) 398.
24. T. H. NOH, M. B. LEE, H. J. KIM and I. K. KANG, *J. Appl. Phys.* **67** (1990) 5568.
25. O. KOHMOTO, K. HANEDA and T. CLOH, *Jpn. J. Appl. Phys.* **29** (1990) L1460.
26. M. FUJINAMI, Y. HASHIGUCHI and T. YAMAMOTO, *ibid.* **29** (1990) L477.
27. J. JIANG, F. AUBERTIN, U. GONSER and H. R. HILZINGER, *Z. Metallkde* **82** (1991) 698.
28. M. KNOBEL, D. R. SANTOS, I. L. TORRIANI and R. S. TURTELLI, *NanoStruct. Mater.* **2** (1993) 399.

Received 3 June 1994
and accepted 3 February 1995